E(adsorbent–Cu_n–ZSM-5) is the total energy of an optimized structure for an adsorbent bound to Cu_n–ZSM-5, *E*(adsorbent) is that of an optimized structure for an adsorbent, and *E*(Cu_n–ZSM-5) is that of an optimized structure for Cu_n–ZSM-5. In the estimation, the $E_{stabilization}$ values were corrected for basis set superposition errors (BSSEs) by using the counterpoise method [36]. Within the B3LYP calculations, the optimized separations between a copper cation and a framework oxygen atom fall in the range of 1.89 to 2.55 Å, being consistent with the previous DFT results [37-44]. The ranges of the calculated Cu–O separations are in good agreement with those obtained from the XRD [45] and EXAFS [46-48] analyses (1.98~2.56 Å). Thus the theoretical method of our choice is appropriate for the present study.

3. Results and Discussion

3.1. ZSM-5 containing monocopper cation (Cu_1–ZSM-5)

3.1.1. The small monocopper zeolite model

First we investigate bindings of an unsaturated hydrocarbon into a monocopper cation bound to a small zeolite framework ($AlSi_2O_4H_8$) for obtaining a baseline for comparison. In the small zeolite model, the monocopper cation is coordinated by two framework oxygen atoms. Using the small zeolite model, we obtained optimized geometries for the binding of an unsaturated hydrocarbon into the monocopper cation, as shown in Figure 2.

Figure 2. (a) Optimized structures for the binding of an unsaturated hydrocarbon ((1) C_2H_2 or (2) C_2H_4) into the monocopper cation bound to the $AlSi_2O_4H_8$ model, and (b) their key orbital interactions.

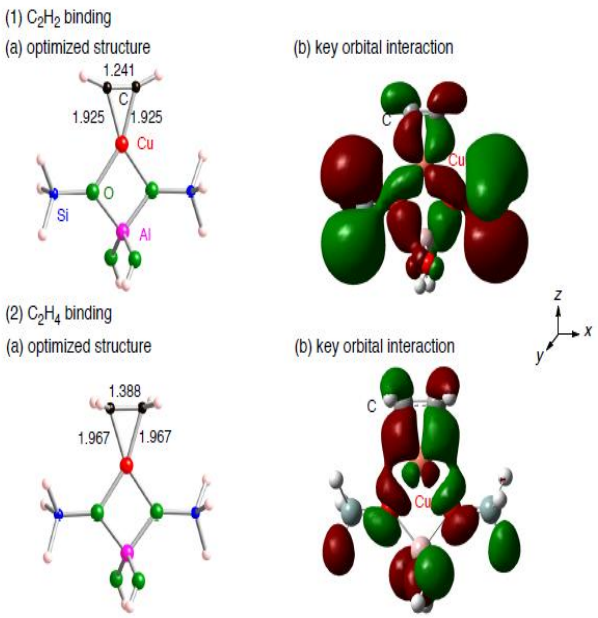

Figure 2 shows that the unsaturated hydrocarbons bind into the monocopper cation in a η^2-bridging fashion. The Cu–C bond lengths were optimized to be 1.925 and 1.967 Å in the acethylene and

ethylene cases, respectively. The optimized structures lie 33 kcal/mol below their dissociation limits toward an unsaturated hydrocarbon and the small zeolite model. The $E_{stabilization}$ values are consistent with those reported in the previous theoretical studies [49-52]. The stabilization mainly comes from in-phase interactions between the d_{xz}(Cu) orbital of the extraframework monocopper and a π* orbital of C_2H_2 or C_2H_4, as shown in Figure 2. Due to the orbital interactions, the Cu(I) cation can donate electrons to the empty π* orbital of an unstaturated hydrocarbon. Accordingly, their CC bonds are activated by the bindings: the optimized CC bond lengths in the acethylene (1.241 Å) and ethylene (1.388 Å) cases are longer than the unperturbed cases by 0.042 Å and 0.061 Å, respectively.

The adsorbed acethylene and ethylene cannot retain liner $D_{\infty h}$ and planar D_{2h} structures, respectively. The geometrical distortions change their vabrational structures. In fact, we see in Tables 1 and 2 that calculated CC stretching vibrational frequencies in the adsorbed acethylene and ethylene are 1793.8 and 1529.4 cm^{-1}, respectively [53]. The values are smaller than those of free acethylene and ethylene (2001.4 and 1645.2 cm^{-1}, respectively). The significant decrease in the CC stretching vibrational frequencies is due to the CC bond activation. Furthermore, their bindings into the extraframework copper cation make CC stretching modes infrared (IR)-active, due to symmetry lowering. Note that CC stretching vibrational modes of free C_2H_4 and C_2H_2 span A_g and Σ_g^+, respectively and thus the modes are IR-inactive [54,55]. Similar symmetry lowering can be seen in the symmetric CH stretching mode in the adsorbed C_2H_2, and thus a new IR peak appears around 3273 cm^{-1} after the C_2H_2 binding into the monocopper cation [56-58].

Table 1. Calculated vibrational frequencies (cm^{-1}) of CC and CH stretching modes of C_2H_2 before and after the binding into the small monocopper zeolite model.

		Free C_2H_2		**C_2H_2 on Cu_1-zeolite**	
	Symmetry	**Frequency**	**IR intensity [a]**	**Frequency**	**IR intensity [a]**
C≡C stretch	Σ_g^+	2001.4	0.00	1793.8	1.12
C–H stretch	Σ_g^+	3400.0	0.00	3273.7	0.40
C–H stretch	Σ_u^+	3300.5	1	3204.0	1

[a] IR intensities are given relative to that of the C–H stretching mode spanning Σ_u^+.

Table 2. Calculated vibrational frequencies (cm^{-1}) of CC and CH stretching modes of C_2H_4 before and after the binding into the small monocopper zeolite model.

		Free C_2H_4		**C_2H_4 on Cu_1-zeolite**	
	Symmetry	**Frequency**	**IR intensity [a]**	**Frequency**	**IR intensity [a]**
C≡C stretch	A_g	1645.2	0.00	1529.4	0.32
C–H stretch	A_g	3036.3	0.00	3023.9	0.00
C–H stretch	B_{3g}	3089.8	0.00	3090.7	0.00
C–H stretch	B_{1u}	3021.3	0.64	3017.7	0.98
C–H stretch	B_{2u}	3117.5	1	3113.2	1

[a] IR intensities are given relative to that of the C–H stretching mode spanning B_{2u}.

3.1.2. Realistic Cu_1–ZSM-5 model

In the previous section (3.1.1), we discussed how an unsaturated hydrocarbon binds into a two-coordinated copper cation by using the small zeolite model. Although we obtained a baseline of the Cu–C bindings, the information is not sufficient to fully understand inner Cu–C interactions in real Cu–ZSM-5 framework due to the variety of the copper coordination environment. The coordination environment should change *d*-splittings of an extraframework copper cation, and therefore the d–π^* interactions are influenced by the copper sites. As a result, the coordination environment should determine the attraction forces operating between the copper cation and an unsaturated hydrocarbon.

Figure 3. Local structures of three optimized structures for a monocopper cation sitting inside the $AlSi_{91}O_{151}H_{66}$ ZSM-5 model. (a) the copper cation sits at the intersection between a straight and a zigzag channel, denoted by **I**. (b) the copper cation sits above a 5-membered ring of a wall along a straight channel, denoted by **5-MR**. (c) the copper cation sits above a 6-membered ring of a wall along a straight channel, denoted by **6-MR**.

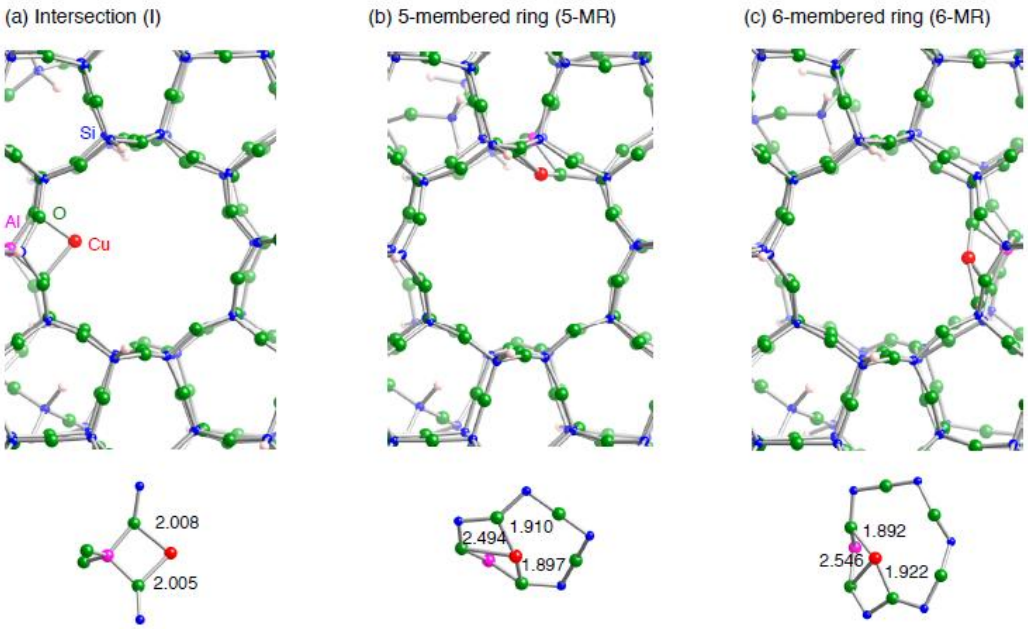

ZSM-5 zeolite has 12 distinguishable tetrahedral(T)-sites in the orthogonal structure. Ref. [37] shows there is no significant difference between the relative energies of ZSM-5 where one Al atom replaces one Si atom in different T-sites. In addition, Nachtigall and Bell separately investigated CO adsorption into Cu–ZSM-5 with one substituted Al atom in different T-sites. Their extensive studies show that the interaction energies between CO and Cu–ZSM-5 as well as CO stretching frequencies change significantly, depending on Cu site types. Also they indicated that the location of the Al atom does not have influence on the binding energies. Judging from the interaction energies, binding sites for an extraframework cation inside ZSM-5 are categorized into three subgroups in Figure 3: one is a cation site near an intersection between a straight and a sinusoidal channels, denoted by **I**, and the others are cations located above a 5-membered and 6-membered rings of a wall along a straight channel, denoted by **5-MR** and **6-MR**, respectively. Along their theoretical findings, we considered

the three binding sites for the Cu cation inside ZSM-5, where the substituted Al atom is located near the cation.

Figure 3 shows that the copper coordination environment in the **I** configuration is similar to that in the small zeolite model: in the **I** configuration, the monocopper cation is bound to two framework oxygen atoms near the substituted Al atom. In contrast, the **5-MR** and **6-MR** configurations have the monocopper cations with a coordination number of 3 [16]. Due to the different copper coordination environment, their electronic configurations are different, as shown in Table 3. The coordination of a Cu(I) cation into ZSM-5 framework results in some degree of the $3d^{10} \rightarrow 3d^9 4s^1$ promotion [41]. In terms of the $3d^{10}$–$3d^9 4s^1$ promotion, there is a slight difference between the **I** and **5-MR** (**6-MR**) configurations: the amount of the 4*s* electron in the **I** configuration (0.25e) is less significant than those in the **5-MR** and **6-MR** configurations (~0.4 e). Since we found the differences in the Cu coordination environments in the three configurations, it is interesting to investigate how the copper coordination environment affects the interactions with an unsaturated hydrocarbon.

Table 3. Electronic configurations of Cu–ZSM-5 before and after the binding of an unsaturated hydrocarbon, based on natural atomic orbital analyses (NPA).

Configuration	Adsorbent	Electronic configuration
I	–	4*s* (0.25) 3*d* (9.84)
	C_2H_2	4*s* (0.36) 3*d* (9.56) 4*p* (0.01)
	C_2H_4	4*s* (0.37) 3*d* (9.57) 4*p* (0.01)
5-MR	–	4*s* (0.42) 3*d* (9.73)
	C_2H_2	4*s* (0.36) 3*d* (9.57) 4*p* (0.01)
	C_2H_4	4*s* (0.36) 3*d* (9.58) 4*p* (0.01)
6-MR	–	4*s* (0.44) 3*d* (9.71)
	C_2H_2	4*s* (0.36) 3*d* (9.55) 4*p* (0.01)
	C_2H_4	4*s* (0.37) 3*d* (9.57) 4*p* (0.01)

Optimized structures for unsaturated hydrocarbons adsorbed on a Cu_1–ZSM-5 model are shown in Figure 4. Table 4 tabulates key parameters for all optimized geometries. We can see in Figure 4 the same types of bindings of the unsaturated hydrocarbons into the copper cation (η^2-fashion), irrespective of different copper coordination environment as well as types of unsaturated hydrocarbon considered. Similar binding fashions have been already reported in Refs. [49-52]. In the η^2-fashion of the C_2H_2 (C_2H_4) bindings, the optimized Cu–C and CC bond lengths are ~1.94 (~1.97) Å and ~1.24 (~1.38) Å, respectively. The CC bonds in the adsorbed unsaturated hydrocarbons are lengthened relative to the free unsaturated hydrocarbons, indicating that the Cu–C bond formation results in the CC bond activation. Interestingly the Cu–C bondings in the η^2-fashion are completely identical to those of the small model. Note that the copper coordination environments in the three configurations are also same after the bindings, in contrast to those before the bindings. Reflecting the same Cu coordination environments, the three models have similar electron configurations of the Cu(I) cation in Table 3. In addition, the amounts of electron transferring (~0.2e) upon the bindings are similar among the three configurations. However, we see slight difference between the **I** and **5-MR** (**6-MR**) configurations in terms of how the electrons transfer between an unsaturated hydrocarbon and Cu–ZSM-5. In the **I** configuration, the 4*s* electron densities increase, whereas the 3*d*

electron densities decrease. Since the two Cu–O bond lengths remain almost unchanged during the binding (Figures 3 and 4), the electron transfer is responsible for the Cu–C bond formation. On the other hand, we can see that both 3*d* and 4*s* orbitals are depopulated upon the bindings in the **5-MR** and **6-MR** configurations. Compared with the **I** configuration, the electron transfers in these configurations originate from not only the formation of the two Cu–O bonds but also significant changes in the copper coordination environments. In fact we see in Figures 3 and 4 that the Cu coordination number changes from 3 to 2, upon the bindings of an unsaturated hydrocarbon into an extraframework copper at **5-MR** or **6-MR** configuration. In contract, such changes in the Cu coordination number are not seen in the **I** configuration.

Figure 4. Local structures of three optimized structures for the binding of an unsaturated hydrocarbon ((1) C_2H_2 or (2) C_2H_4) into a monocopper cation embedded inside the $AlSi_{91}O_{151}H_{66}$ ZSM-5 model. (a) the copper cation sits at the intersection between a straight and a zigzag channel, denoted by **I**. (b) the copper cation sits above a 5-membered ring of a wall along a straight channel, denoted by **5-MR**. (c) the copper cation sits above a 6-membered ring of a wall along a straight channel, denoted by **6-MR**. Optimized bond lengths are in Å. The $E_{stabilization}$ values are in kcal/mol.

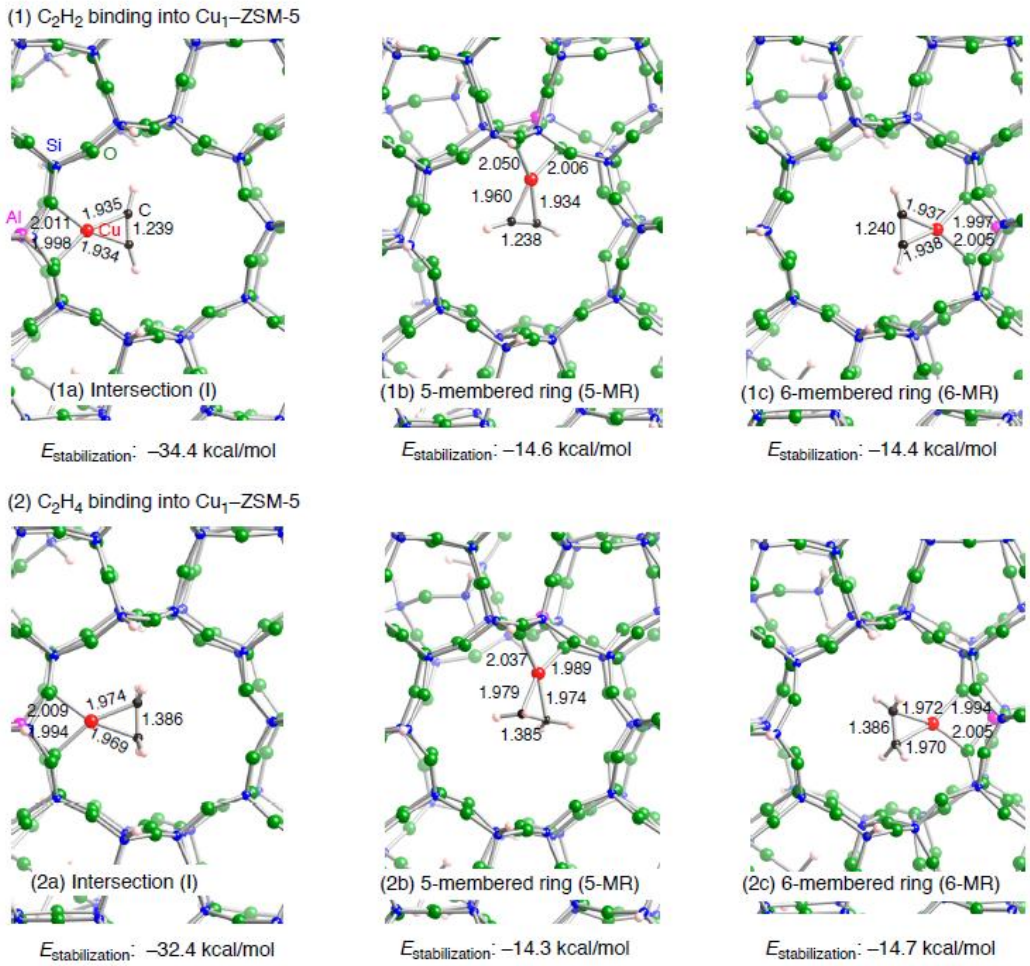

Despite the same binding types in the three configurations, the stabilization energies depend on their copper coordination environment: the calculated $E_{stabilization}$ values in the **I** configuration (–34.4 (C_2H_2) and –32.4 (C_2H_4) kcal/mol) are more pronounced than those in the **5-MR** configuration (–14.6 (C_2H_2) and –14.3 (C_2H_4) kcal/mol) and the **6-MR** configuration (–14.4 (C_2H_2) and –14.7 (C_2H_4) kcal/mol). The stabilization energies in the **I** configuration are almost the same as those in the small zeolite models, whereas those in the **5-MR** and **6-MR** configurations are different. The different $E_{stabilization}$ values are also associated with the changes in the copper coordination environments upon the bindings. Here we consider quantitatively why the copper coordination environment plays an essential role in determining the stabilization energies. In general, an extraframework cation shifts from its original position by approaching of an adsorbent to the cation. The cation shifts destabilize a zeolite structure itself. The destabilization by the cation shifts counteracts direct attractive interactions between an extraframework cation and an adsorbent. Thus the balance between the destabilization by the cation shifts and the stabilization by the direct interactions determines a stable conformation of an adsorbent inside a zeolite. The importance of the balance has been already discussed by Nachtigall and coworkers [59,60]. We can see dependences of the destabilization on the copper coordination environment in Table 4, where the destabilization energies *E*(deform) are listed. The *E*(deform) values are defined by *E*(deformed Cu–ZSM-5) – *E*(adsorbent-free Cu–ZSM-5). Here *E*(deformed Cu–ZSM-5) is the single-point-energy of a deformed Cu–ZSM-5 taken from an optimized adsorbent–Cu–ZSM-5 complex, and *E*(adsorbent-free Cu–ZSM-5) is the total energy of an optimized adsorbent-free Cu–ZSM-5 structure. Positive *E*(deform) values indicate that a Cu–ZSM-5 itself is destabilized by the inner coordination bond formation. Table 4 indicates strong site-dependencies of the *E*(deform) values.

Table 4. Key parameters of the optimized structures for an unsaturated hydrocarbon adsorbed on a dicopper active center embedded inside a realistic ZSM-5 model.

Configuration [a]	Adsorbent	Binding mode	Cu–C [b]	CC [b]	$E_{stabilization}$ [c]	*E*(deform) [d]
I	C_2H_2	η^2	1.934, 1.935	1.239	–34.4	2.6
5MR	C_2H_2	η^2	1.934, 1.960	1.238	–14.6	20.4
6MR	C_2H_2	η^2	1.937, 1.938	1.240	–14.4	22.5
I	C_2H_4	η^2	1.969, 1.974	1.386	–32.4	2.3
5MR	C_2H_4	η^2	1.974, 1.979	1.385	–14.3	17.8
6MR	C_2H_4	η^2	1.970, 1.972	1.386	–14.7	20.3

[a] Configuration: I is the intersection site, 5MR and 6MR are the 5- and 6-membered sites.; [b] Bond lengths in Å.; [c] $E_{stabilization}$ in kcal/mol.; [d] *E*(deform) in kcal/mol.

In fact the *E*(deform) values in the **I** configuration (2.6 (C_2H_2) and 2.3 (C_2H_4) kcal/mol) are negligible relative to those in the **5-MR** configuration (20.4 (C_2H_2) and 17.8 (C_2H_4) kcal/mol) and the **6-MR** configuration (22.5 (C_2H_2) and 20.3 (C_2H_4) kcal/mol). The site-dependent *E*(deform) values are reasonable, because decreasing the copper coordination number in the **5-MR** and **6-MR** configurations loses attractive Cu–O interactions at some extent. Taking the different *E*(deform) values into account, we can understand that bindings of an unsaturated hydrocarbon to the monocopper cation in the **I** configurations are energetically favorable over those in the **5-MR** and **6-MR** configurations. Note that

the deformation energies are more significant than those in the interaction with NO molecule (the *E*(deform) values are 1 and 8 kcal/mol for intersection and channel wall sites, respectively [41]). The larger *E*(deform) values suggest that the η^2-bindings require larger displacement of copper cations rather than the η^1-bindings. In this situation we demonstrated from DFT calculations that the copper coordination environment is a key factor determining the bindings of an unsaturated hydrocarbon into an extraframework monocopper cation of ZSM-5.

3.2. ZSM-5 containing dicopper active center (Cu_2–ZSM-5)

In this section we will focus on an unsaturated hydrocarbon bound to a dicopper active center embedded in ZSM-5. In this situation, configurations of the two copper cations within a ZSM-5 cavity may be responsible for the unsaturated hydrocarbon bindings, in addition to their copper coordination environment. Experimentally the presence of Cu pairs in ZSM-5 was demonstrated by using extended X-ray absorption fine structure (EXAFS) [61-63] spectroscopy and X-ray power diffraction [45] studies. To fully understand behaviors of an unsaturated hydrocarbon inside a ZSM-5 cavity, it is indispensable to clarify how configurations of the two copper cations inside ZSM-5 affect the properties of adsorbed unsaturated hydrocarbons.

3.2.1. The small dicopper zeolite model

First we use a small zeolite model containing the dicopper active center ($[Cu–AlSi_2O_4H_8]_2$) to increase our preliminary understanding of the interactions with an unsaturated hydrocarbon. Using the small dicopper zeolite model, we optimized an unsaturated hydrocarbon adsorbed on the dicopper active center, except for the Cu•••Cu separation ($S_{Cu•••Cu}$). Potential energy surfaces of the approaching of an unsaturated hydrocarbon into the dicopper active center are seen in Figure 5 as a function of $S_{Cu•••Cu}$. Figure 5 shows their stabilization energies $E_{stabilization}$' defined as $-E$(adsorbent) $-E$(Cu_2–zeolite[$S_{Cu•••Cu}$]) + E(adsorbent–Cu_2–zeolite[$S_{Cu•••Cu}$]), where E(adsorbent) is the total energy of the optimized structure for an adsorbent, E(adsorbent–Cu_2–zeolite[$S_{Cu•••Cu}$]) is that of an optimized structure for an adsorbent bound to the small dicopper zeolite at a certain $S_{Cu•••Cu}$ value, and E(Cu_2–zeolite[$S_{Cu•••Cu}$]) is that of a Cu_2–zeolite taken from the optimized adsorbent–Cu_2–zeolite[$S_{Cu•••Cu}$] structure. When $S_{Cu•••Cu}$ is 6 Å, C_2H_2 or C_2H_4 binds into one copper cation bound to the $AlSi_2O_4H_8$ zeolite model. Then the optimized structures for the C_2H_2 and C_2H_4 bindings are, respectively, 35.6 and 37.2 kcal/mol stable relative to those in the dissociation limits toward an unsaturated hydrocarbon and the free small zeolite model with the two copper cations apart by 6 Å. Of course, the $E_{stabilization}$' values are close to those obtained in the small monocopper zeolite.

Decreasing the Cu•••Cu separation, two Cu–C bonds are newly generated. As a result, an unsaturated hydrocarbon binds into both copper cations in a μ-η^2: η^2 fashion. Because of the new Cu–C bond formation, the $E_{stabilization}$' values lower significantly until a certain $S_{Cu•••Cu}$ value. In fact we see in Figure 5 that the potential energy surface of the C_2H_2–dicopper (C_2H_4–dicopper) complex has one local minimum at $S_{Cu•••Cu}$ of 2.888 (3.735) Å.

Figure 5. (a) Potential energy surfaces of approaching of an unsaturated hydrocarbon (C_2H_2 or C_2H_4) into the smaller dicopper zeolite model ($[Cu–Al_1Si_3O_4H_8]_2$). $E_{stabilization}$' is plotted as a function of the Cu•••Cu separation. (b) optimized structures for the binding of an unsaturated hydrocarbon ((1) C_2H_2 or (2) C_2H_4) into the small dicopper zeolite model.

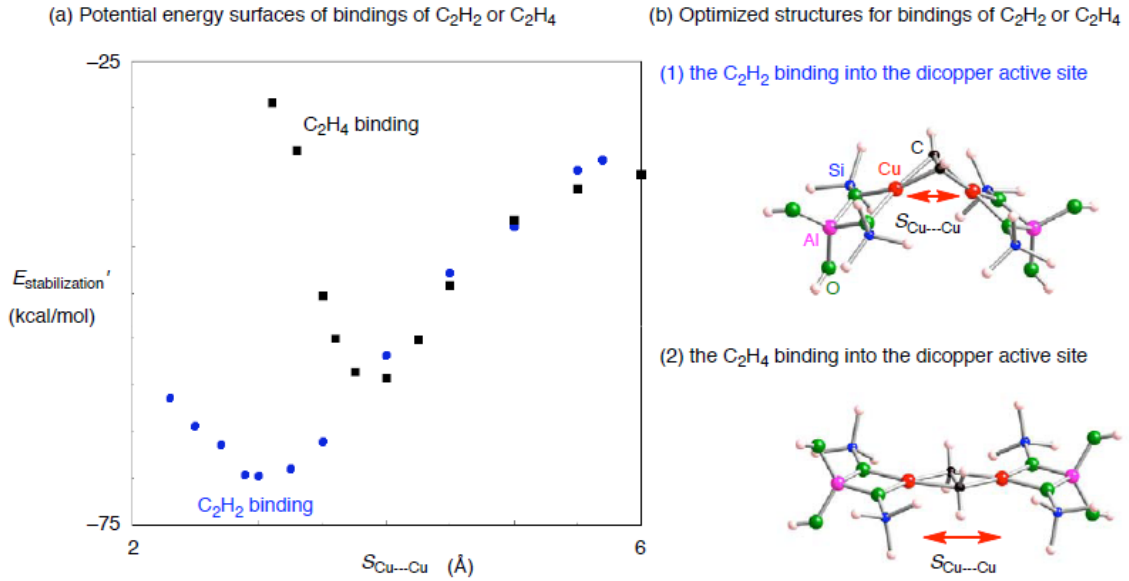

As shown in Figure 5 and Table 5 the optimized C_2H_2– and C_2H_4–dicopper complexes lie, respectively, 34.0 and 21.4 kcal/mol below the structures with the $S_{Cu•••Cu}$ values of ~6 Å. These DFT results clearly show that the interactions of acethylene with the dicopper active center are more significant than the ethylene case. The differences between the acethylene and ethylene additions are unique in the dicopper cases, which cannot be seen in the monocopper cases. Moreover, we can see some discrepancy in the optimized structures between the acathylene and ethylene cases: the optimized C_2H_2–Cu_2–zeolite contains a μ-η^2: η^2 Cu_2C_2 core with a butterfly form, whereas the C_2H_4–Cu_2–zeolite contains a planar μ-η^2: η^2 core. Reflecting the structural differences, the C_2H_2–Cu_2–zeolite has a smaller $S_{Cu•••Cu}$ value than that in C_2H_4–Cu_2–zeolite.

Table 5. Key parameters of the optimized structures of an unsaturated hydrocarbon adsorbed onto a dicopper active center bound to a small zeolite model.

Adsorbent	Binding mode	Cu–C[a]	CC[a]	$S_{Cu•••Cu}$[b]	$E_{stabilization}$',[c]
C_2H_2	μ–η^2: η^2	1.932, 1.933 1.933, 1.934	1.297	2.888	–69.6
C_2H_4	μ–η^2: η^2	2.003, 2.003, 2.003, 2.003	1.449	3.735	–58.6

[a] Bond lengths in Å.; [b] $S_{Cu•••Cu}$ is the Cu•••Cu separation in Å.; [c] $E_{stabilization}$' in kcal/mol.

Whether the Cu_2C_2 core has a planar or a butterfly structure can be confirmed by their IR spectra, especially their CC stretching vibrational modes (Tables 6 and 7). We see in Tables 6 and 7 that CC stretching vibrational frequencies were calculated to be 1557.1 and 1469.4 cm^{-1} in C_2H_2 and C_2H_4 adsorbed on the dicopper active center, respectively. Lower CC stretching frequencies than those in

the monocopper model are ascribed to more significant CC bond activation by the dicopper active center: the optimized CC bond lengths in the acethylene and ethylene additions are 1.297 and 1.449 Å, respectively (see Table 5). More importantly, the CC stretching vibrational mode in the acethylene addition is IR-active, whereas that in the ethylene addition is IR-inactive due to the planarity of its Cu_2C_2 core. The calculated IR data will help to determine how an unsaturated hydrocarbon binds into a dicopper active center embedded inside ZSM-5.

Table 6. Calculated vibrational frequencies (cm^{-1}) of CC and CH stretching modes of C_2H_2 before and after the binding into the small dicopper zeolite model.

	Free C_2H_2			**C_2H_2 on Cu_2-zeolite**	
	Symmetry	**Frequency**	**IR intensity[a]**	**Frequency**	**IR intensity[a]**
C≡C stretch	Σ_g^+	2001.4	0.00	1557.1	1.44
C–H stretch	Σ_g^+	3400.0	0.00	3170.0	0.90
C–H stretch	Σ_u^+	3300.5	1	3127.8	1

[a] IR intensities are given relative to that of the C–H stretching mode spanning Σ_u^+.

Table 7. Calculated vibrational frequencies (cm^{-1}) of CC and CH stretching modes of C_2H_4 before and after the binding into the small dicopper zeolite model.

	Free C_2H_4			**C_2H_4 on Cu_2-zeolite**	
	Symmetry	**Frequency**	**IR intensity [a]**	**Frequency**	**IR intensity [a]**
C≡C stretch	A_g	1645.2	0.00	1469.4	0.00
C–H stretch	A_g	3036.3	0.00	3004.9	0.00
C–H stretch	B_{3g}	3089.8	0.00	3085.4	0.00
C–H stretch	B_{1u}	3021.3	0.64	3001.8	17.10
C–H stretch	B_{2u}	3117.5	1	3100.5	1

[a] IR intensities are given relative to that of the C–H stretching mode spanning B_{2u}.

3.2.2. Realistic Cu_2–ZSM-5 model

In section 3.2.1, we used the small dicopper zeolite model, and found differences between the dicopper and monocopper cations in terms of the interactions with an unsaturated hydrocarbon. Next we turn to dicopper active centers located in a 10-MR cavity of the realistic ZSM-5 model $Al_2Si_{90}O_{151}H_{60}$. Since copper cations usually sit near the Al substituted positions, the locations of the double $Si \rightarrow Al$ substitution within the ZSM-5 framework control the configurations of a dicopper active center. Here we consider four locations of the double substitution in Figure 6: the **2NN**, **3NN**, **4NN**, and **5NN** configurations contain the Al pairs being, respectively second, third, fourth, and fifth nearest-neighbors with respect to tetrahedral sites contained in the 10-MR. Using the different configurations of the Al pair, their initial geometries were constructed by placing each Cu apart by ~2.0 Å from two oxygen atoms bound to a substituted Al atom. After the B3LYP optimization, four configurations of the dicopper center inside ZSM-5 were obtained, as shown in Figure 6. The Cu•••Cu separation in Cu_2–ZSM-5 decreases in the order **5NN** (6.442 Å) > **4NN** (6.370 Å) > **3NN** (2.561 Å) > **2NN** (2.372 Å). The Cu•••Cu separations in the **2NN** and **3NN** configurations are close to those

obtained by EXAFS analyses (2.47–3.13 Å). In the optimized Cu_2–ZSM-5 structures, each Cu cation coordinates into two or three framework oxygen atoms. The Cu•••Cu separations are out of the range of a suitable span between the two copper cations into which an unsaturated hydrocarbon preferentially binds in a μ-η^2: η^2-fashion (Figure 5). Note that the formation of Cu pairs in the **3NN** and **2NN** configurations is consistent with the Spuhler's findings [38] by means of a combined quantum mechanics/interatomic potential function technique(QM-pot).

Taking varying Cu•••Cu separations by locations of the double Si → Al substitution into account, we discuss how an unsaturated hydrocarbon binds into a dicopper active center. Figure 7 shows the optimized structures for an unsaturated hydrocarbon adsorbed on a dicopper active center embedded in a ZSM-5 model, whose key parameters are listed in Table 8. We can see in Figure 7 and Table 8 two types of binding of C_2H_2 into a dicopper active center. In the **2NN** configuration, C_2H_2 binds into the dicopper active center in a μ-η^1: η^1 fashion, whereas the **3NN**, **4NN**, and **5NN** configurations have a μ-η^2: η^2 Cu_2C_2 core. In the **3NN**, **4NN**, and **5NN** configurations, the Cu•••Cu separations were optimized to be 3.047, 3.236, and 3.315 Å, respectively. These $S_{Cu\cdots Cu}$ values are close to the separation between the two copper cations into which C_2H_2 binds in a μ-η^2: η^2 fashion in Figure 5. The significant differences in the $S_{Cu\cdots Cu}$ values between before and after the C_2H_2 binding ($\Delta S_{Cu\cdots Cu}$) indicate that two copper cations significantly shift after the binding. In contrast, the **2NN** configuration does not have a room, and thus the two copper cations cannot move to positions suitable for the C_2H_2 binding in a μ-η^2: η^2 fashion. Instead, the **2NN** configuration adopts the μ-η^1:η^1 binding fashion with a stabilization energy of –33.7 kcal/mol. Surprisingly the $E_{stabilization}$ value is comparable to that of the **3NN** configuration (–35.8 kcal/mol), despite the different C_2H_2 binding fashions.

Figure 6. Local structures of four optimized Cu_2–ZSM-5 structures where the ZSM-5 framework was modeled as a $Al_2Si_{90}O_{151}H_{66}$ cluster. The four types of optimized structures can be distinguished by positions of double Si → Al substitution: the two substituted Al atoms within a ten-membered ring are second nearest neighbor (**2NN**), third nearest neighbor (**3NN**), fourth nearest neighbor (**4NN**), and fifth nearest neighbor (**5NN**). Optimized bond lengths are given in Å.

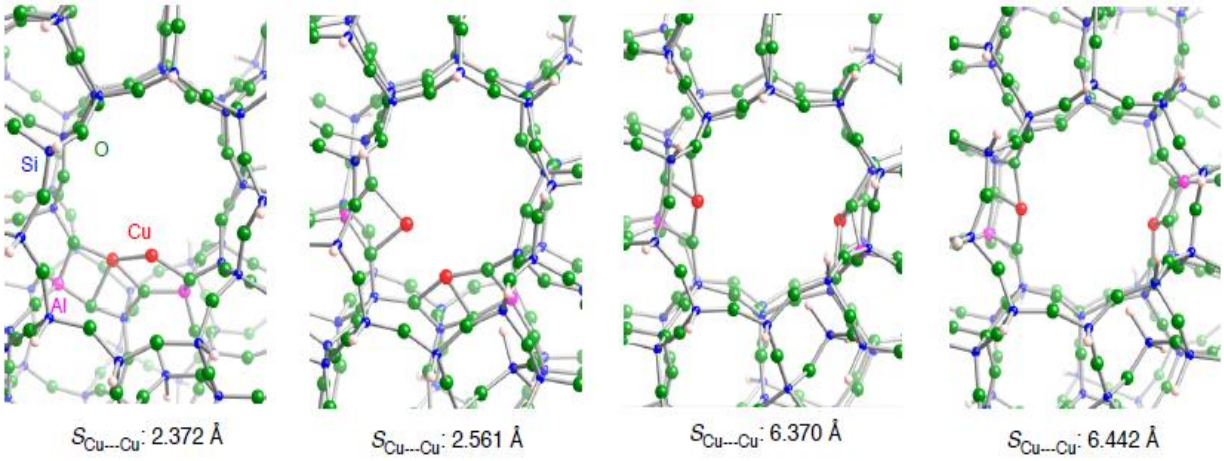

Figure 7. Local structures of four optimized structures for the binding of an unsaturated hydrocarbon ((1) C_2H_2 or (2) C_2H_4) into a dicopper active center embedded inside the $Al_2Si_{90}O_{151}H_{66}$ ZSM-5 model. The four types of optimized structure can be distinguished by positions of double Si → Al substitution: the two substituted Al atoms within a ten-membered ring are (a) second nearest neighbor (**2NN**), (b) third nearest neighbor (**3NN**), (c) fourth nearest neighbor (**4NN**), and fifth nearest neighbor (**5NN**). Optimized bond lengths together with the Cu•••Cu separations are given in Å. The $E_{stabilization}$ values are in kcal/mol.

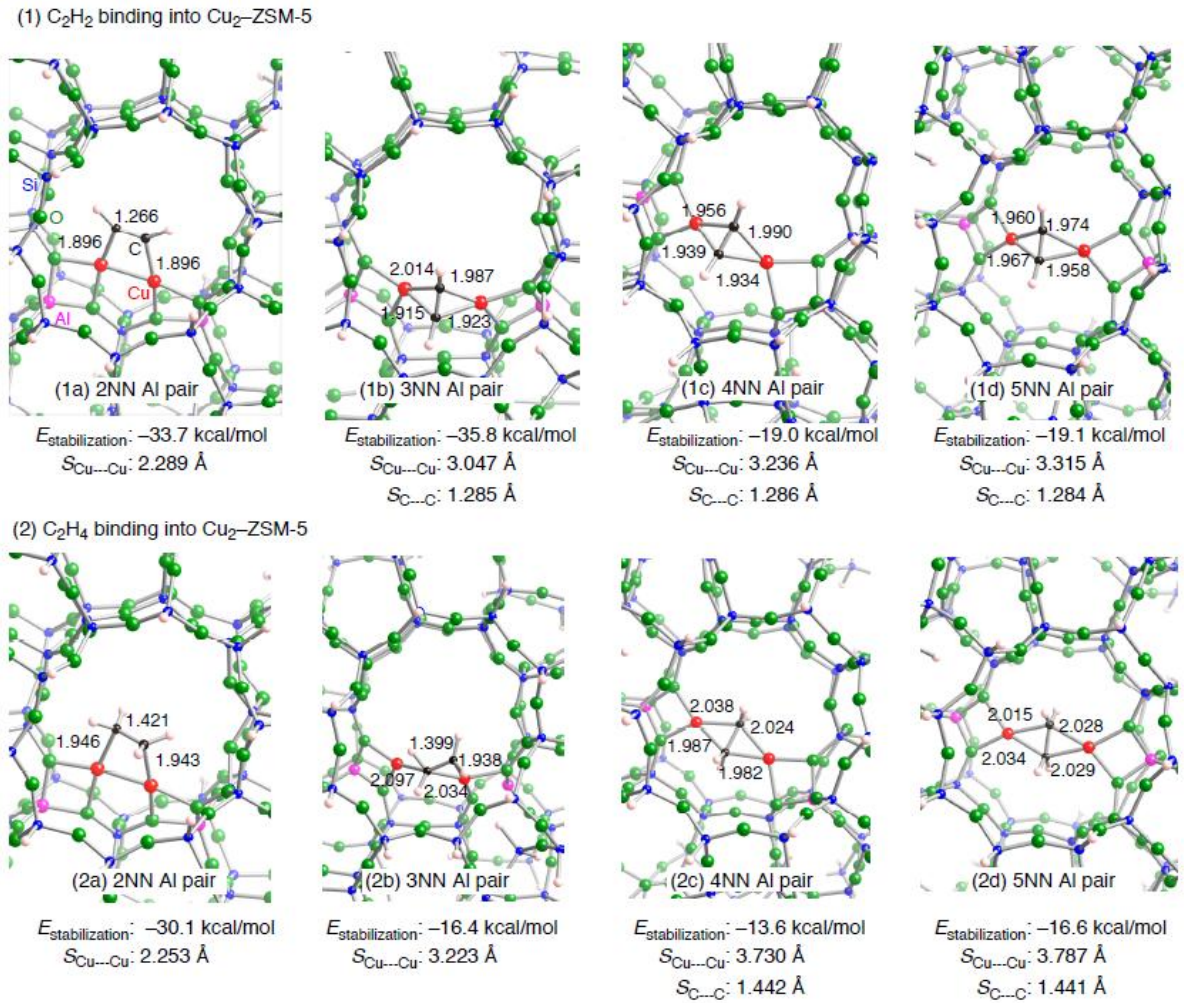

In the above discussion, we found that whether the two copper cations smoothly shift determines a preferable C_2H_2 binding fashion in a ZSM-5 cavity. Although the importance of the copper shifts can be also seen in the monocopper case, the *E*(deform) values in the dicopper cases (Table 8) are more pronounced than those in the monocopper cases. In addition, we found from Table 8 strong dependences of the *E*(deform) values on the dicopper configurations: the *E*(deform) values decrease in the following order: **5NN** ≈ **4NN** > **3NN** > **2NN**. The decrease in the *E*(deform) values has a close relation to the $\Delta S_{Cu\cdots Cu}$ values. Table 8 shows that the $\Delta S_{Cu\cdots Cu}$ values decrease in the order **4NN** ≈ **5NN** > **3NN** > **2NN**, suggesting that the C_2H_2 bindings in the **5NN** and **4NN** configurations cause two copper cations to shift significantly, compared with those in the **3NN** and **2NN**

configurations. Therefore, the dependent *E*(deform) values are understandable. Reflecting the *E*(deform) values, the stabilization in the **4NN** and **5NN** configurations is less significant than that in the **3NN** configuration, because the destabilization by the cation shifts diminishes the attraction by the direct interactions. Thus the variety of the Cu–C bonding characters is unique in the restricted environment of ZSM-5.

Table 8. Key parameters of the optimized structures of an unsaturated hydrocarbon adsorbed onto a dicopper active center embedded inside a realistic ZSM-5 model.

Configuration [a]	Adsorbent	Binding mode	Cu–C [b]	CC [b]	$S_{Cu\cdots Cu}$ [c] ($\Delta S_{Cu\cdots Cu}$ [d])	$E_{stabilization}$ [e]	E(deform) [f]
2NN	C_2H_2	μ–η^1: η^1	1.896, 1,896	1.266	2.289 (–0.083)	–33.7	19.0
3NN	C_2H_2	μ–η^2: η^2	1.915, 1.923, 1.987, 2.014	1.285	3.047 (0.486)	–35.8	24.7
4NN	C_2H_2	μ–η^2: η^2	1.934, 1.939, 1.956, 1.990	1.286	3.236 (–3.134)	–19.0	45.7
5NN	C_2H_2	μ–η^2: η^2	1.958, 1.960, 1.967, 1.974	1.284	3.315 (–3.127)	–19.1	47.2
2NN	C_2H_4	μ–η^1: η^1	1.946, 1.943	1.421	2.253 (–0.119)	–30.1	18.0
3NN	C_2H_4	μ–η^1: η^2	1.938, 2.034, 2.097	1.399	3.223 (0.662)	–16.4	25.5
4NN	C_2H_4	μ–η^2: η^2	1.982, 1.987, 2.024, 2.038	1.442	3.730 (–2.640)	–13.6	41.9
5NN	C_2H_4	μ–η^2: η^2	2.015, 2.028, 2.029, 2.034	1.441	3.787 (–2.655)	–16.6	43.1

[a] Configuration: The **2NN**, **3NN**, and **4NN** configurations have Al pairs being second-, third-, and fourth nearest neighbors within a ten-membered ring of the ZSM-5 model, respectively.; [b] Bond lengths in Å.; [c] $S_{Cu\cdots Cu}$ is the Cu•••Cu separation in Å.; [d] $\Delta S_{Cu\cdots Cu}$ is the difference in the Cu•••Cu separation between before and after the binding of an unsaturate hydrocarbon.; [e] $E_{stabilization}$' in kcal/mol.; [f] E(deform) in kcal/mol.

Compared with the C_2H_2 bindings, more complicated binding modes are found in the C_2H_4 bindings into a dicopper center in Figure 7: the **2NN** configuration has a μ-η^1:η^1 form, the **3NN** configuration has a μ-η^1:η^2 form, and the **4NN** and **5NN** configurations have a μ-η^2:η^2 form. The calculated $E_{stabilization}$ values are close to those obtained experimentally (–15.4 and –21.4 kcal/mol) [64]. The μ-η^2:η^2 binding fashions in the **4NN** and **5NN** configurations are similar to that obtained in the small zeolite model: in both cases, the Cu and C atoms virtually lie in a plane. The Cu•••Cu separations in the **4NN** and **5NN** configurations (3.730 and 3.787 Å, respectively) are essentially identical to the equilibrium separation between C_2H_4 and the small zeolite model (3.735 Å in Figure 5), and thus the similarity in the binding fashion is reasonable. In contrast, the optimized $S_{Cu\cdots Cu}$ values in the **2NN** and **3NN** configurations are 1.482 and 0.512 Å smaller than the equilibrium

separation in the small dicopper zeolite model. Accordingly these configurations cannot adopt a μ-η^2:η^2 binding fashion. Note that the μ-η^1:η^2 binding fashion (**3NN**) is an intermediate between the μ-η^1:η^1 (**2NN**) and μ-η^2:η^2 (**4NN** and **5NN**) fashions. How C_2H_4 binds into a dicopper active center inside ZSM-5 is also followed by the balance rule. As shown in Table 8, destabilization of the Cu_2–ZSM-5 by the C_2H_4 binding is similar to that by the C_2H_2 binding form a viewpoint of energetics. However, direct interactions by the C_2H_4 binding are 11.0 kcal/mol weaker than those by the C_2H_2 binding (see Table 5). Compared with the C_2H_2 bindings, the importance of the destabilization by the cation shifts to determine a preferable C_2H_4 binding fashion is more effective rather than the direct attractive C_2H_4–dicopper interactions.

4. Conclusions

We found from large-scale DFT calculations that characters of copper–carbon bonds formed inside ZSM-5 change significantly, depending on its copper coordination environment. Actually attractive interactions of an unsaturated hydrocarbon with a two-coordinated extraframework copper cation are significant relative those with a higher-coordinated copper cation. The dependences of the interactions are related with shifts of a copper cation accompanied by the bindings: the shift of a cation with a higher coordination number costs energy a lot. Thus site-preferences of two-coordinated copper cations as the unsaturated-hydrocarbon binding site are reasonable. When an unsaturated hydrocarbon binds into an embedded dicopper active center, configurations of the two copper cations are important to determine the bindings, in addition to its coordination environment. Because of the different interactions between an unsaturated hydrocarbon and a mono- or dicopper copper active center, various binding fashions (η^2, μ-η^1:η^1, μ-η^1:η^2, and μ-η^2:η^2 fashions) are expected in Cu–ZSM-5. The variety of characters of the copper–carbon bonds is unique in the restricted environment of a zeolite.

Acknowledgements

Support by Grants-in Aid for Scientific Research from the Ministry of Education, Cluture, Sports, Science, and Technology of Japan (No. 21655021).

References and Notes

1. Crabtree, R.H. *The Organometallic Chemistry of the Transtion Metals*, 2nd ed.; John Wiley & Son, Inc.: New York, NY, USA, 1994.
2. Crabtree, R.H. The organometallic chemistry of alkanes. *Chem. Rev.* **1985**, *85*, 245–269.
3. Bergman, B.G. C–H activation. *Nature* **2007**, *446*, 391–393.
4. Arndtsen, B.A.; Bergman, B.G.; Mobley, T.A.; Peterson, T.H. Selective intermolecular carbon-hydrogen bond activation by synthetic metal complexes in homogeneous solution. *Acc. Chem. Res.* **1995**, *28*, 154–162.
5. Schröder, D.; Schwarz, H. C-H and C-C bond activation by bare transition-metal oxide cations in the gas phase. *Angew. Chem. Int. Ed. Engl.* **1995**, *34*, 1973–1995.
6. Eller, K.; Schwarz, H. Organometallic chemistry in the gas phase. *Chem. Rev.* **1991**, *91*, 1121–1177.

7. Weisshaar, J.C. Bare transition metal atoms in the gas phase: reactions of M, M^+, and M^{2+} with hydrocarbons. *Acc. Chem. Res.* **1993**, *26*, 213–219.
8. Trost, B.M. On inventing reactions for atom economy. *Acc. Chem. Res.* **2002**, *35*, 695–705.
9. Hahn, C. Enhancing electrophilic alkene activation by increasing the positive net charge in transition-metal complexes and application in homogeneous catalysis. *Chem. Eur. J.* **2004**, *10*, 5888–5899.
10. Shriver, D.F.; Atkins, P.W. *Inorganic Chemistry*, 4th ed.; Oxford University Press: Oxford, UK, 2006.
11. Yumura, T.; Kertesz, M.; Iijima, S. Local modifications of single-wall carbon nanotubes induced by bond formation with encapsulated fullerenes. *J. Phys. Chem. B* **2007**, *111*, 1099–1109.
12. Yumura, T.; Kertesz, M. Cooperative behaviors in carbene additions through local modifications of nanotube surfaces. *Chem. Mater*. **2007**, *19*, 1028–1034.
13. Yumura, T.; Kertesz, M.; Iijima, S. Confinement effects on site-preferences for cycloadditions into carbon nanotubes. *Chem. Phys. Lett.* **2007**, *444*, 155–160.
14. Yumura, T.; Takeuchi, M.; Kobayashi, H.; Kuroda, Y. Effects of ZSM-5 zeolite confinement on reaction intermediates during dioxygen activation by enclosed dicopper cations. *Inorg. Chem.* **2009**, *48*, 508–517.
15. Itadani, A.; Sugiyama, H.; Tanaka, M.; Ohkubo, T.; Yumura, T.; Kobayashi, H.; Kuroda, Y. Potential for C−H Activation in CH_4 Utilizing a CuMFI-Type Zeolite as a Catalyst. *J. Phys. Chem. C* **2009**, *113*, 7213–7222.
16. Yumura, T.; Yamashita, H.; Torigoe, H.; Kobayashi, H.; Kuroda, Y. Site-specific Xe addition into Cu–ZSM-5 zeolite. *Phys. Chem. Chem. Phys.* **2010**, *12*, 2392–2400.
17. Iwamoto, M.; Furukawa, H.; Mine, Y.; Uemura, F.; Mikuriya, S.; Kagawa, S. Copper(II) ion-exchanged ZSM-5 zeolites as highly active catalysts for direct and continuous decomposition of nitrogen monoxide. *J. Chem. Soc., Chem. Commun.* **1986**, 1272–1273.
18. Kuhn, P.; Pale, P.; Sommer, J.; Louis, B. Probing Cu-USY zeolite reactivity: design of a green catalyst for the synthesis of diynes. *J. Phys. Chem. C* **2009**, *113*, 2903–2910.
19. Yu, J.-S.; Kevan, L. Effects of reoxidation and water vapor on selective partial oxidation of propylene to acrolein in copper(II)-exchanged X and Y zeolites. *J. Phys. Chem.* **1991**, *95*, 6648–6653.
20. Becke, A.D. Density-functional exchange-energy approximation with correct asymptotic behavior. *Phys. Rev. A* **1988**, *38*, 3098–3100.
21. Becke, A.D. Density-functional thermochemistry. III. The role of exact exchange. *J. Chem. Phys*. **1993**, *98*, 5648–5652.
22. Stephens, P.J.; Devlin, F.J.; Chabalowski, C.F.; Frisch, M.J. Ab initio calculation of vibrational absorption and circular dichroism spectra using density functional force fields. *J. Phy. Chem.* **1994**, *98*, 11623–11627.
23. Lee, C.; Yang, W.; Parr, R.G. Development of the Colle-Salvetti correlation-energy formula into a functional of the electron density. *Phys. Rev. B* **1988**, *37*, 785–789.
24. Vosko, S.H.; Wilk, L.; Nusair, M. Accurate spin-dependent electron liquid correlation energies for local spin density calculations: a critical analysis. *Can. J. Phys.* **1980**, *58*, 1200–1211.

25. Frisch, M.J.; Trucks, G.W.; Schlegel, H.B.; Scuseria, G.E.; Robb, M.A.; Cheeseman, J.R.; Montgomery, J.A., Jr.; Vreven, T.; Kudin, K.N.; Burant, J.C.; *et al.* Gaussian 03. Gaussian, Inc.: Pittsburgh, PA, USA, 2003.
26. The ZSM-5 structure was taken from the Cerius 2 database. Accerys, Software, Inc.: San Diego, CA, USA, 2001.
27. Krishnan, R.; Binkley, J.S.; Seeger, R.; Pople, J.A. Self-consistent molecular orbital methods. XX. A basis set for correlated wave functions. *J. Chem. Phys.* **1980**, *72*, 650–654.
28. Wachters, A.J.H. Gaussian basis set for molecular wavefunctions containing third-row atoms. *J. Chem. Phys.* **1970**, *52*, 1033–1036.
29. Hay, R.J. Gaussian basis sets for molecular calculations. The representation of 3d orbitals in transition-metal atoms. *J. Chem. Phys.* **1977**, *66*, 4377–4384.
30. Hehre, W.J.; Ditchfield, R.; Pople, J.A. Self—Consistent Molecular Orbital Methods. XII. Further Extensions of Gaussian—Type Basis Sets for Use in Molecular Orbital Studies of Organic Molecules. *J. Chem. Phys.* **1972**, *56*, 2257–2261.
31. Francl, M.M.; Pietro, W.J.; Hehre, W.J.; Binkley, J.S.; Gordon, M.S. Self-consistent molecular orbital methods. XXIII. A polarization-type basis set for second-row elements. *J. Chem. Phys.* **1982**, *77*, 3654–3665.
32. Hariharan, P.C.; Pople, J.A. The influence of polarization functions on molecular orbital hydrogenation energies. *Theor. Chim. Acta* **1973**, *28*, 213–222.
33. Binkley, J.S.; Pople, J.A.; Hehre, W.J. Self-consistent molecular orbital methods. 21. Small split-valence basis sets for first-row elements. *J. Am. Chem. Soc.* **1980**, *102*, 939–947.
34. Gordon, M.S.; Binkley, J.S.; Pople, J.A.; Pietro, W.J.; Hehre, W.J. Self-consistent molecular-orbital methods. 22. Small split-valence basis sets for second-row elements. *J. Am. Chem. Soc.* **1982**, *104*, 2797–2803.
35. Pietro, W.J.; Francl, M.M.; Gordon, M.S.; Hehre, W.J.; Defrees, D.J.; Pople, J.A.; Binkley, J.S. Self-consistent molecular orbital methods. 24. Supplemented small split-valence basis sets for second-row elements. *J. Am. Chem. Soc.* **1982**, *104*, 5039–5048.
36. Boys, S.F.; Bernardi, F. The calculation of small molecular interactions by the differences of separate total energies. Some procedures with reduced errors. *Mol. Phys*. **1970**, *19*, 553–566.
37. Nachtigallová, D.; Nachtigall, P.; Sierka, M.; Sauer, J. Coordination and siting of Cu^+ ions in ZSM-5: A combined quantum mechanics/interatomic potential function study. *Phys. Chem. Chem. Phys.* **1999**, *1*, 2019–2026.
38. Spuhler, P.; Holthausen, M.C.; Nachtigallová, D.; Nachtigall, P.; Sauer, J. On the Existence of CuI Pairs in ZSM-5 - A Computational Study. *Chem. Eur. J.* **2002**, *8*, 2099–2115.
39. Davidová, M.; Nachtigallová, D.; Bulánek, R.; Nachtigall, P. Characterization of the Cu^+ sites in high-silica zeolites interacting with the CO molecule: combined computational and experimental Study. *J. Phys. Chem. B* **2003**, *107*, 2327–2332.
40. Bulánek, R.; Silhan, M.; Nachtigallová, D.; Nachtigall, P. Calculations of site-specific CO stretching frequencies for copper carbonyls with the "near apectroscopic accuracy": CO interaction with Cu^+/MFI. *J. Phys. Chem. A* **2003**, *107*, 10381–10388.

41. Davidová, M.; Nachtigallová, D.; Nachtigall, P.; Sauer, J. Nature of the Cu^{+}–NO Bond in the Gas Phase and at Different Types of Cu^{+} Sites in Zeolite Catalysts. *J. Phys. Chem. B* **2004**, *108*, 13674–13682.
42. Bludský, O.; Silhan, M.; Nachtigall, P.; Bucko, T.; Benco, L.; Hafner, J. Theoretical Investigation of CO Interaction with Copper Sites in Zeolites: Periodic DFT and Hybrid Quantum Mechanical/Interatomic Potential Function Study. *J. Phys. Chem. B* **2005**, *109*, 9631–9638.
43. Bulánek, R.; Drobná, H.; Nachtigall, P.; Rubeš, M.; Bludský, O. On the site-specificity of polycarbonyl complexes in Cu/zeolites: combined experimental and DFT study. *Phys. Chem. Chem. Phys.* **2006**, *8*, 5535–5542.
44. Zheng, X.; Zhang, Y.; Bell, A.T. Density Functional Theory Study of CO Adsorption on Cu(I)-ZSM-5. *J. Phys. Chem. C* **2007**, *111*, 13442–13451.
45. Mentzen, B.F.; Bergeret, G. Crystallographic Determination of the Positions of the Copper Cations in Zeolite MFI. *J. Phys. Chem. C* **2007**, *111*, 12512–12516.
46. Kumashiro, R.; Kuroda, Y.; Nagao, M. New analysis of oxidation state and coordination environment of copper ion-exchanged in ZSM-5 Zeolite. *J. Phys. Chem. B* **1999**, *103*, 89–96.
47. Kuroda, Y.; Kumashiro, R.; Yoshimoto, T.; Nagao, M. Characterization of active sites on copper ion-exchanged ZSM-5-type zeolite for NO decomposition reaction. *Phys. Chem. Chem. Phys.* **1999**, *1*, 649–656.
48. Kuroda, Y.; Yagi, K.; Horiguchi, N.; Yoshikawa, Y.; Kumashiro, R.; Nagao, M. New light on the state of active sites in CuZSM-5 for the NO decomposition reaction and N_2 adsorption. *Phys. Chem. Chem. Phys.* **2003**, *5*, 3318–3327.
49. Hüber, G.; Rauhut, G.; Stoll, H.; Roduner, E. Ethyne adsorbed on CuNaY zeolite: FTIR spectra and quantum chemical calculations. *J. Phys. Chem. B* **2003**, *107*, 8568–8573.
50. Hüber, G.; Rauhut, G.; Stoll, H.; Roduner, E. FTIR measurements and quantum chemical calculations of Ethylene adsorbed on CuNaY. *Phys. Chem. Chem. Phys.* **2002**, *4*, 3112–3121.
51. Broclawik, E.; Rejmak, P.; Kozyra, P.; Datka, J. DFT quantum chemical modeling of the interaction of alkenes with Cu^{+} sites in zeolites. *Catal. Today* **2006**, *114*, 162–168.
52. Rejmak, P.; Mitoraj, M.; Broclawik, E. Electronic view on ethene adsorption in Cu(I) exchanged zeolites. *Phys. Chem. Chem. Phys.* **2010**, *12*, 2321–2330.
53. Calculated vibrational frequencies were scaled by 0.9659, along the following reference.: Halls, M.D.; Velkovski, J.; Schlegel, H.B. Harmonic frequency scaling factors for Hartree-Fock, S-VWN, B-LYP, B3-LYP, B3-PW91 and MP2 with the Sadlej pVTZ electric property basis set. *Theor. Chem. Acc.* **2001**, *105*, 413–421.
54. Herzberg, G. *Molecular Spectra and Molecular Structure: Infrared and Raman Spectra of Polyatomic Molecules*; Krieger Publishing com.: Malabar, FL, USA, 1991.
55. Willian, K.R.; Ewing, E. Infrared spectra and structures of ethene on NaCl(100). *J. Phys. Chem.* **1995**, *99*, 2186–2193.
56. Datka, J.; Kukulska-Zając, E.; Kobyzewa, W. The activation of acetylene by Cu^{+} ions in zeolites studied by IR spectroscopy. *Catal. Today* **2005**, *101*, 123–129.
57. Datka, J.; Kukulska-Zając, E. IR studies of the activation of C=C bond in alkenes by Cu^{+} ions in zeolites. *J. Phys. Chem. B* **2004**, *108*, 17760–17766.

58. Itadani, A.; Yumura, T.; Ohkubo, T.; Kobayashi, H.; Kuroda, Y. Existence of dual species composed of Cu^+ in CuMFI being bridged by C_2H_2. *Phys. Chem. Chem. Phys.* **2010**, submitted.
59. Nachtigallová, D.; Bludsky, O.; Areán, C.O.; Bulánek, R.; Nachtigall, P. The vibrational dynamics of carbon monoxide in a confined space–CO in zeolites. *Phys. Chem. Chem. Phys.* **2006**, *8*, 4849.
60. Nachtigall, P.; Bulánek, R. Theoretical investigation of site-specific characteristics of CO adsorption complexes in the Li^+-FER zeolite. *Appl. Catal., A* **2006**, *307*, 118–127.
61. Palomino, G.T.; Fisicaro, P.; Bordiga, S.; Zecchina, A.; Giamello, E.; Lamberti, C. Oxidation states of copper ions in ZSM-5 zeolites. a multitechnique investigation. *J. Phys. Chem. B* **2000**, *104*, 4064–4073.
62. Hamada, H.; Matsubayashi, N.; Shimada, H.; Kintaichi, Y.; Ito, T.; Nishijima, A. XANES and EXAFS analysis of copper ion-exchanged ZSM-5 zeolite catalyst used for nitrogen monoxide decomposition. *Catal. Lett.* **1990**, *5*, 189–196.
63. Grünert, W.; Hayes, N.W.; Joyner, R.W.; Shpiro, E.S.; Siddiqui, M.R.H.; Baeva, G.N. Structure, chemistry, and activity of Cu-ZSM-5 catalysts for the selective reduction of NOx in the presence of oxygen. *J. Phys. Chem.* **1994**, *98*, 10832–10846.
64. Borgard, G.D.; Molvik, S.; Balaraman, P.; Root, T.W.; Dumesic, J.A. Microcalorimetric and infrared spectroscopic studies of CO, C_2H_4, N_2O, and O_2 adsorption on Cu-Y zeolite. *Langmiur* **1995**, *11*, 2065–2070.